The current issue and full text archive of this journal is available at
www.emeraldinsight.com/0961-5539.htm

Numerical simulation of pulsatile turbulent flow in tapering stenosed arteries

Bin Xiao and Yuwen Zhang
Department of Mechanical and Aerospace Engineering, University of Missouri, Columbia, Missouri, USA

Received 30 October 2006
Revised 17 June 2008
Accepted 17 June 2008

Abstract

Purpose – The purpose of this paper is to investigate the geometric effects and pulsatile characteristics during the stenotic flows in tapering arteries.

Design/methodology/approach – The low Reynolds number $k-\omega$ turbulence model is applied to describe the stenotic flows in the tapering arteries in this paper. The results are divided into two sections. The first section characterizes the geometric effects on the turbulent flow under steady condition. The second section illustrates the key physiological parameters including the pressure drop and wall stress during the periodic cycle of the pulsatile flow in the arteries.

Findings – The tapering and stenoses severity intensify the turbulent flow and stretch the recirculation zones in the turbulent arterial flow. The wall shear stress, pressure drop and velocity vary most intensively at the peak phase during the periodic cycle of the pulsatile turbulent flow.

Originality/value – This paper provides a comprehensive understanding of the spatial-temporal fluid dynamics involved in turbulent and transitional arterial flow with stenoses. The low Reynolds number $k-\omega$ turbulence model method is applied for the analyses of the geometric effects on the arterial flow and fluid feature during the periodic cycle.

Keywords Heart, Pulsating flow, Turbulent flow, Simulation, Fluid dynamics
Paper type Research paper

Nomenclature

I = turbulence intensity
k = turbulent kinetic energy (m^2/s^2)
p = pressure (N/m^2)
Re = Reynolds number
T = time period (s)
u = velocity (m/s)
w = oscillation frequency (*rad/s*)
ε = turbulent energy dissipation rate (m^2/s^3)
μ = dynamic viscosity (kg/m-s)
ρ = density (kg/m^3)
τ_{ij} = Reynolds stress tensor ($kg/m\text{-}s^2$)
ω = specific dissipation rate (ε/k)

Subscripts

i, j = Cartesian components
k = relative to turbulent kinetic energy
0 = relative to origin
m = gradient amplitude
t = relative to turbulence

Introduction

Arteriosclerosis is a common heart attack and stroke disease in the industrialized world due to excess sedentary and rich food. Arteriosclerosis in the carotid artery obstructs blood flow to the brain and stimulates the formation of stenoses. Arterial hemodynamics plays an important role in pathogenesis analysis of arterioscleroses,

International Journal of Numerical Methods for Heat & Fluid Flow
Vol. 19 No. 5, 2009
pp. 561-573

0961-5539
DOI 10.1108/09615530910963526

most of which are associated with abnormal blood flow in stenotic arteries. Stenotic flow is inherently pulsatile due to the cyclic nature of the heart pump, which will generate turbulence with low Reynolds number. In the blood flow, the typical Reynolds number range varies from 1 in small arterioles to approximately 4,000 in the largest artery, the aorta (Ku, 1997). In the presence of sufficiently severe stenoses during the cardiac cycle, the transition to turbulence flow was found in the downstream of stenoses (Roshko, 1954; Stein and Sabbah, 1976). Pulsatility also creates a periodic generation of turbulence, the temporarily turbulent flow was observed at Reynolds numbers as low as 400 even in a circular tube without stenosis during the deceleration of a pulsating flow (Winter and Nerem, 1984). Turbulence influences many physiological processes with its effects on the pressure drop and wall shear stress in stenotic arteries (Giddens *et al.*, 1993). Therefore, experimental and computational studies of stenotic blood flow are of interest among bioengineers and medical researchers. Ahmed (1998) reported an experimental investigation of pulsatile flow in a smooth stenosis. Ojha *et al.* (1989) studied flow through constricted tubes using a photochromic technique. Gidden and co-workers (Deshpande and Giddens, 1980; Ahmed and Giddens, 1983a, b, 1984; Lieber and Giddens, 1990) constructed pulsatile flow models in blood vessels, and measured velocities and wall shear stress using laser Doppler velocimetry. Marshall *et al.* (2004) measured the time-resolved velocity using magnetic resonance imaging and calculated the wall shear stress vectors. Experimental results were compared qualitatively with the corresponding computational fluid dynamics (CFD) predictions. The results show that, in the stenosed phantom, flow in the bulb region of the internal carotid artery was concentrated along the outer wall with low flow recirculation near the inner wall. And the converse with low flow was found near the out wall of the bulb in the normal phantom.

The experimental analysis of complex flows, particularly those that are pulsatile and transitional, is both labor-intensive and expensive. With the advance of computer speed and the increasing resolution and complexity of numerical simulation, CFD have begun to play a major role in improving our understanding of biofluid flows in general and blood flow in arteries in particular (Ku, 1997; Berger and Jou, 2000). There have been several recent studies to examine the turbulence structure in low-Reynolds number stenotic flows. The steady simulations were performed by Ghalichi *et al.* (1998) and Lee *et al.* (2003), both reported results using Wilcox $k - \omega$ model turbulence model for simulations of flow through straight tubes with stenoses. Both groups found that the $k - \omega$ model to be suitable when compared to the experimental data obtained by Ahmed and Giddens (1983a, b) and Deshpande and Giddens (1980). Scotti and Piomelli (2001a, b) conducted direct numerical simulation and large eddy simulations (LES), Reynolds averaged Navier-Stokes (RANS) simulations of pulsatile turbulent channel flow subjected to an unsteady pressure gradient. The results showed that the fluctuations generated in the near-wall region are restricted to a certain distance from the wall, depending on the oscillation frequency. Mittal *et al.* (2001) applied LES to investigate the pulsatile flow model through a simple arterial stenosis, the flow downstream of the stenosis transitions to turbulence and exhibits all the classic feature of post-stenosis flow described by former results. Varghese and Frankel (2003) conducted numerical modeling of turbulent flow in stenosed tubes by FLUENT using a variety of two-equation turbulence models (three variants of the $k - \varepsilon$ model and the transitional $k - \omega$ model). It was found that the low-Re transitional $k - \omega$ model was in agreement with the experimental measurement results by Ojha *et al.* (1989) and Ahmed and Giddens (1983a). Jung *et al.* (2006) performed a multiphase transient non-

Newtonian three dimensional CFD simulation for pulsatile flow in an idealized curved section of a human coronary artery. They correlated the lower wall shear stress with the outside curvature by introducing the effect of red blood cells. These predictions provided insight into how blood-borne particulates interact with artery walls. Li *et al.* (2007) investigate the flow field and stress field for different degrees of axisymmetric cosine shape stenoses with varying diameter reduction of 30, 50 and 70 percent, respectively. The turbulence model with the consideration of fluid-structure and realistic boundary conditions was developed. Taber *et al.* (2007) applied the commercial software (Comsol Multiphysics) to explore the transition from peristaltic to pulsatile flow in the embryonic heart tube. This study illustrated the interrelationship between form and function in the early embryonic heart. Nguyen *et al.* (2008) quantified the risk of atherogensis based on the average wall shear stress on pulsatile blood utilizing the software package FLUENT. They analyzed the effects of internal carotid artery angles, off-plane angles and the symmetric bifurcations on the wall shear stress and the risk of vascular disease.

As tapering is a significant aspect of arterial systems in mammals and human beings; present study will focus on the pulsating flow through tapering stenosed arteries. Wilcox's low-Re transitional $k-\omega$ model has been chosen for current simulation because, as noted above, it has been reported to be successful in predicting transitional flows at low Reynolds number (Wilcox, 1993). More details on Wilcox's $k-\omega$ models can be found in books on turbulent flows and modeling (Wilcox, 1993; Pope, 2000). Since the development of arteriosclerosis reduces the elastic property of the arterial wall, it is reasonable to assume the arterial wall is rigid in current study. The fluid is considered incompressible and Newtonian in consistence with most experimental studies. The flow features include strong wall shear stress, recirculation and turbulence in the arterial flow with stenoses, which have substantial effects on the hemodynamics and potentially therefore the evolution of the plaque, such as arteriosclerosis. To gain a comprehensive understanding of the spatial-temporal fluid dynamics involved in the stenotic fluid flow, this paper utilizes the numerical method for the analysis of turbulent and transitional blood flow in a tapering artery with stenoses.

Turbulence models

Figure 1 shows a schematic diagram for pulsatile blood flow in a tapering stenotic artery. Due to the axisymmetry with respect to the centerline, the calculation will be conducted on only half of the domain using the low Reynolds number $k-\omega$ turbulence model. The RANS equations represent transport equations for the mean flow quantities, with the consideration of the effect of turbulent eddies. The instantaneous flow variables in the Navier-Stokes equations such as velocity, u, can be written as the sum of an average value, $\bar{u}$, and a fluctuation about the value, u'. Other scalar variables

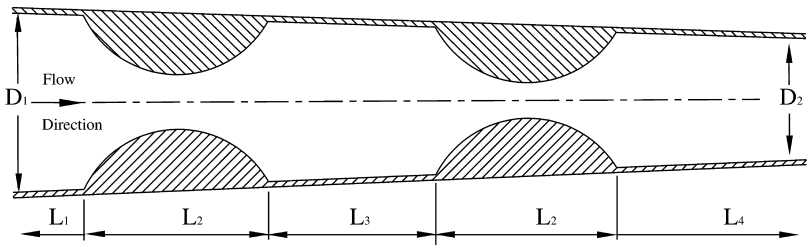

Figure 1.
Physical model for pulsatile flow in a tapering stenosed artery

such as pressure can be described in the same form. Applying this decomposition to the Navier-Stokes equations yields the RANS equations. The governing equations for the blood flow in the tapering stenotic arterial segment can be written as:

$$\frac{\partial \bar{u}_i}{\partial x_i} = 0 \tag{1}$$

$$\rho \frac{D\bar{u}_i}{Dt} = -\frac{\partial \bar{p}}{\partial x_i} + \frac{\partial}{\partial x_j}\left[\mu\left(\frac{\partial \bar{u}_i}{\partial x_j} + \frac{\partial \bar{u}_j}{\partial x_i}\right) - \overline{\rho u_i u_j}\right] \tag{2}$$

where $D()/Dt = \partial()/\partial t + u_j[\partial()/\partial x_j]$ and μ is the dynamic viscosity.

As seen above, averaging the momentum equations gives rise to a new term known as Reynolds stress tensor, $-\overline{\rho u_i u_j}$. It represents the time-averaged rate of momentum transfer due to turbulence that can be expressed as

$$-\overline{\rho u_i u_j} \approx \mu_t\left(\frac{\partial \bar{u}_i}{\partial x_j} + \frac{\partial \bar{u}_j}{\partial x_i}\right) = \tau_{ij} \tag{3}$$

where μ_t is the turbulent eddy viscosity. A two-equation $k-\omega$ turbulence model can be used to model the cross correlations which arise from the nonlinear terms in the governing equations and thereby close the equations. The eddy viscosity is modeled as:

$$\mu_t = \frac{\rho k}{\omega} \tag{4}$$

And the turbulent transport equation for kinetic energy and turbulence dissipation can be described as:

$$\rho \frac{Dk}{Dt} = \frac{\partial}{\partial x_j}\left[(\mu + \sigma^* \mu_t)\frac{\partial k}{\partial x_j}\right] - \tau_{ij}\frac{\partial \bar{u}_i}{\partial x_j} + \rho\beta^* k\omega \tag{5}$$

$$\rho \frac{D\omega}{Dt} = \frac{\partial}{\partial x_j}\left[(\mu + \sigma\mu_t)\frac{\partial \omega}{\partial x_j}\right] - \alpha\frac{\omega}{k}\tau_{ij}\frac{\partial \bar{u}_i}{\partial x_j} + \rho\beta\omega^2 \tag{6}$$

where $\sigma^* = 0.5, \beta^* = 0.072, \sigma = 0.5, \alpha = 1.0,$ and $\beta = 0.072$ (Wilcox, 1993). The standard $k-\omega$ model is described by Equations (3)-(6) combined with the given coefficients.

The low Reynolds number $k-\omega$ model has a transitional variant, because the flow is not fully turbulent in the entire domain or throughout the entire pulse cycle. The low Reynolds number $k-\omega$ model is similar to the standard model except for some modifications. The key modification is the low-Re correction factor applied to the eddy viscosity (Wilcox, 1993)

$$\mu_t = \alpha^* \frac{\rho k}{\omega} \tag{7}$$

which influences the entire model by appearing in the momentum and turbulence equations. The low-Re correction factor is derived from

$$\alpha^* = \alpha^*_\infty \left(\frac{\alpha^*_0 + \mathrm{Re}_t/R_k}{1 + \mathrm{Re}_t/R_k} \right), \mathrm{Re}_t = \frac{\rho k}{\mu \omega} \tag{8}$$

where $R_k = 6.0, \alpha^*_0 = 0.024$, and $\alpha^*_\infty = 1.0$ (Wilcox, 1993). This factor varies from 0-1 and influences the turbulence model based on the local flow structure. The transport equations for k and ω remains as in Equations (5) and (6), except with the addition of the low-Re correction in the eddy viscosity and the modification of some coefficients to make them functions of the local flow structure. In the equation for turbulent kinetic energy, the coefficient on the dissipation term is described as

$$\beta^* = \beta^*_\infty \left(\frac{4/15 + (\mathrm{Re}_t/R_\beta)^4}{1 + (\mathrm{Re}_t/R_\beta)^4} \right) \tag{9}$$

where $R_\beta = 8$ and $\beta^*_\infty = 0.09$ (Wilcox, 1993). The production coefficient for turbulent dissipation equation is calculated from

$$\alpha^* = \frac{\alpha_\infty}{\alpha^*} \left(\frac{\alpha_0 + \mathrm{Re}_t/R_\omega}{1 + \mathrm{Re}_t/R_\omega} \right) \tag{10}$$

where $R_\omega = 2.95, \alpha_\infty = 0.52, \alpha_0 = 1/9$ (Wilcox, 1993). For the time periodic calculation, the time period, T, was calculated in terms of the oscillation frequency, w, as $T = 2\,\pi/w$. The time step was then calculated by dividing the time period with the number of iterations required for convergence during each step. The temporally periodic boundary condition at the inlet of the artery can be written as:

$$u = u_0 + u_m \sin(wt) \tag{11}$$

where u_0 is the mean velocity and u_m is the velocity gradient amplitude. The turbulence boundary condition at the inlet can be described as

$$k = \frac{3}{2}(u_0 I)^2, \varepsilon = \frac{0.09\, k^2}{\beta^* \nu} \tag{12}$$

$$I = 0.16\ \mathrm{Re}^{-\frac{1}{8}}, \mathrm{Re} = \frac{\rho u_0 H}{\mu} \tag{13}$$

At the outlet cross section, we assume the flow field has no change, that is

$$\frac{\partial u_i}{\partial x_i} = 0 \tag{14}$$

Since the arterial walls are assumed to be no-slip, the velocity at the wall can be written as

$$u_i = 0 \tag{15}$$

Numerical solution

Our numerical algorithm utilizes the finite volume method with the collocated variable arrangement to solve two-dimensional, RANS Equations described by Equations (1)-(15). The meshing is conducted by applying boundary-fitted non-orthogonal meshing technique (see Figure 2). Since the grid lines follow the boundaries, the boundary conditions are more easily implemented than with stepwise approximation of curved boundaries. Convective terms in the momentum and turbulence equations were descretized using a first-order upwind scheme. A first-order temporal discretization scheme was used for all transient calculations. The mass-momentum equations were solved in a segregated manner using the simple algorithm and all results were converged to residual of less than 10^{-4}, normalized using the inlet mean velocity.

When the Favre variables are used for the expansions of the variables and Reynolds averaging is applied, the RANS equations have the same form as the laminar equations provided the molecular viscosity, μ, is replaced by the effective viscosity $\mu_{eff} = \mu + \mu_t$. However, as the time scale associated with the turbulence is much shorter than that connected with the mean flow, the equations for the $k - \omega$ model are much stiffer than the laminar flow. For this reason, in the numerical solution procedure, an outer iteration of the momentum and pressure equations in which the value of the eddy viscosity is based on the value of k and ω at the end of the preceding iteration is firstly performed. After this has been completed, an outer iteration of the turbulent kinetic energy and dissipation equations is made. Since these equations are highly non linear, they have to be linearized prior to iteration. After completing the iteration of the turbulence model equations, we are ready to recalculate the eddy viscosity and start a new outer iteration. An important consideration for turbulence modeling is near-wall treatment, which can be performed by using the wall function approach (Wilcox, 1993).

The computational domain is half of the artery because of its axisymmetry. The grids consist of 240×20 four-noded volumes. The meshing density is relatively heavy around the stenoses since the boundary-fitted non-orthogonal meshing technique is employed. To check for grid independence, the grid resolution was increased by a factor of two in all the directions. The fluid flow case with 75 percent stenoses was repeated and the difference in the velocity profile was less than 5 percent with the finer mesh. We utilize a very small time-step $\Delta t = 10^{-4}$ in order to ensure the convergence for pulsatile flow case. Steady simulation typically required 1,000 iterations for convergence, whereas transient simulation typically required 800 iterations per time-step. The present study first considers steady flow to analyze the effect of tapering and stenosis on the velocity field and pressure distribution of the artery. Pulsatile simulations are then performed to analyze the temporal centerline velocity, pressure distribution and wall shear stress, which are the key factors of incidence of the arteriosclerosis.

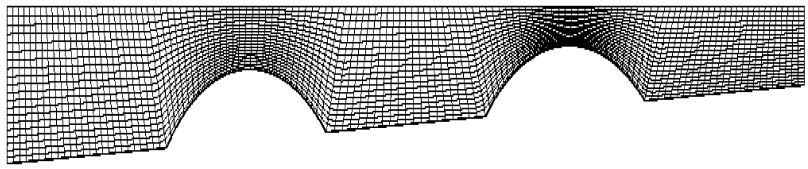

Figure 2.
Two-dimensional view of the mesh in the vicinity of the stenoses

Result and discussion

In order to validate the low Reynolds number $k-\omega$ turbulence model, steady flow computation result is compared to the experiment data by Ahmed and Giddens (1983a) at different axial locations distal to the smooth stenosis and inlet Re equals to 500. Figure 3 shows a reasonable agreement with the experimental data. Though this study mainly concerns the simulation of pulsatile flow through stenosed arteries, it is more efficient by first considering the steady flows through constricted arteries to investigate the effects of stenotic severity and tapering on the turbulent flow. Then the unsteady case will be performed for better understanding the pulsatile flow in a certain artery. During the computational procedure, we used the characteristic parameters: $D_1 = 3.2$ mm, $D_2 = 0.5D_1$, $L_1 = 2D_1$, $L_2 = L_3 = 1.2D_1$, $L_4 = 4D_1, u_0 = 0.5$ m/s, $u_m = 0.25$ m/s, $\rho = 1.056 \times 10^3$ kg/m^3, $\mu = 4.03 \times 10^{-3}$ kg/m-s, $w = 3.14$ rad/s and $T = 0.4$ s.

In Figure 4 the dimensionless mean horizontal velocity (u/u_0) profile in the vicinity of the 75 percent and 90 percent area reduction stenoses is plotted. The same inlet velocity profile, $u_0 = 0.5$ m/s, was specified for both cases. The maximum velocity $u_{\max}$ reaches 1.444 m/s for the 75 percent stenoses case and reaches 4.18 m/s for the 90 percent stenoses case at the throat of the second stenosis. For the 75 percent stenoses case, the velocity profiles at the upstream of the stenoses and at a certain distance from the second stenosis are positive, while at the downstreams of the stenoses the velocity profiles show a reverse flow near the arterial walls. When the severity of the stenoses increases to 90 percent, even at the upstream of the second stenosis and at certain distance from the second stenosis, the reverse flow appears. Compared with the two arterial flows with different severity of stenoses, when the severity of stenoses increases, the reverse flow trend is enhanced, and the centerline velocity also increases.

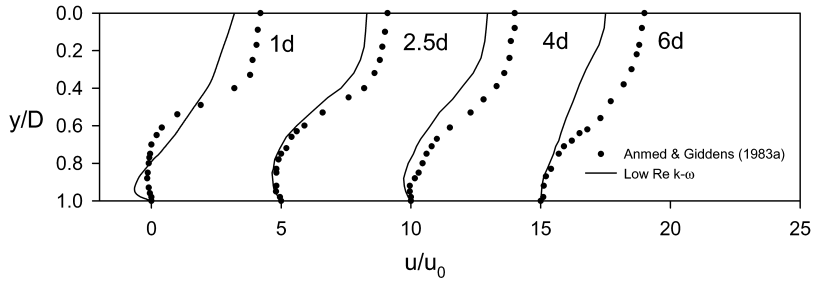

Figure 3.
Velocity profile comparison of the computational results and experimental data

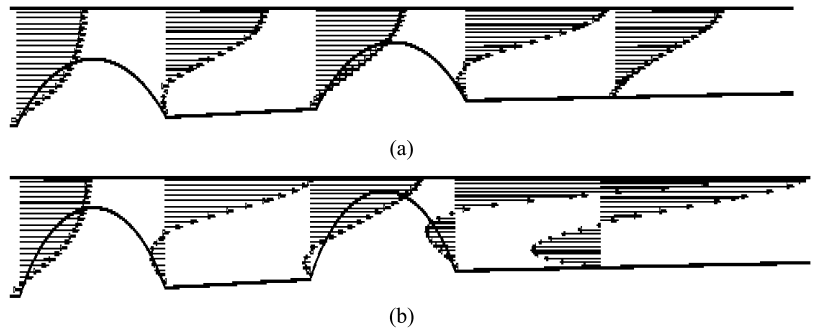

Figure 4.
Comparison of the velocity profiles with different stenoses: (a) 75 percent stenoses, (b) 90 percent stenoses

Figure 5 shows the streamlines of the flow fields in the vicinity of the 75 percent and 90 percent stenoses. The recirculation vortices are founded downstreams of the stenoses. It is clear that flow separation is closely related to stenosis severity and the separation region is much greater for more severe stenosis. This is of clinic interest because the separation region is related to cell residence time and plaque growth (Cao and Rittgers, 1998).

Figure 6 illustrates the contour of pressure distributions for in the vicinity of the 75 percent and 90 percent stenoses. The pressure decreases dramatically across the throat, and then increases after stenoses to the outlet pressure. The pressure at the throat of the first stenosis is -0.183 kPa, and drops to -0.516 kPa at the throat of the second stenosis for the caser with 75 percent stenoses. The contour lines of the pressures become dense near region with the severe stenoses which means the rapid variation of the pressures and causes compressive stress in the artery. As can be seen from Figure 6, the pressure varies more strongly with more severe stenoses.

In order to estimate the effect of tapering on the fluid flow in the artery, the velocity profiles and the streamlines of fluid flow with/without tapering are plotted in Figures 7 and 8. The maximum velocity u_{max} is 1.008 m/s for the flat artery and becomes 4.18 m/s for the tapering artery. It can be seen from Figure 7, due to the effects of tapering and the flow area reduction, the velocity increases more rapidly from the wall to the centerline in the tapering artery than that happened in the flat artery. Both reverse flows and positive flows in the tapering artery are seen to get considerably steeper compared with what occurs in the flat artery. Additionally, the recirculation zones present downstream of the stenoses in the tapering artery are seen to grow compared with that happened in the flat artery as can be seen from Figure 8.

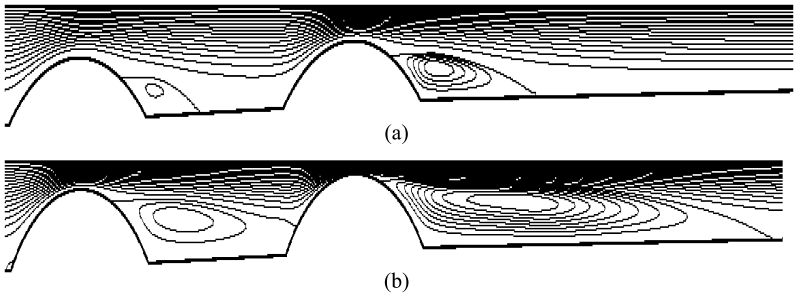

Figure 5.
Comparison of the streamlines of the flow fields with different stenoses:
(a) 75 percent stenoses,
(b) 90 percent stenoses

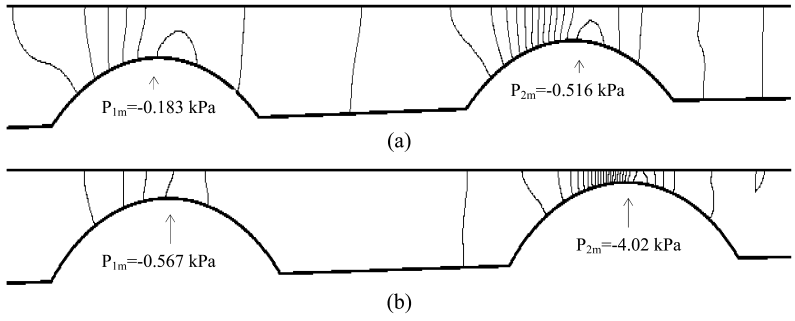

Figure 6.
Comparison of pressure distribution with different stenoses:
(a) 75 percent stenoses,
(b) 90 percent stenoses

Turbulent pulsatile flow

Figure 9 shows the centerline velocity profiles for the 90 percent stenoses case when $t = 2.2$ s (accelerate phase), $t = 2.5$ s (peak phase), and $t = 3.2$ s (decelerate phase). Of the three times, as expected, the maximum velocity is seen to occur at the peak phase and occurs just downstream of the second stenosis midpoint. In Figure 8, centerline velocity increases slowly at the area before the first stenosis at all three times, and increases rapidly upstream of the first stream because of the sharp reduction of flow area. The centerline velocity peaks at the throat of the first stenosis. And then decreases when the area increases downstream of the first stenosis. The similar phenomenon happens when the fluid flows through the second stenosis, and velocity increases/decreases more rapidly upstream/downstream compared with that happened at the first stenosis.

As mentioned earlier, it has been considered that the distribution and magnitude of the pressure and the wall shear stress on the arterial channels play important roles in the genesis and acceleration of arterial disease. For instance, local hypertension may be directly caused by localized increase in lateral wall pressure (Holman, 1955). It has also been established that the sites of predilection for atherosclerosis are often correlated with regions of low shear stress (Ku *et al.*, 1985; Friedman *et al.*, 1981). Figure 10 shows the centerline pressure distribution for the 90 percent constriction case. As can be seen, the pressure falls to the lowest level at the peak phase during the period cycle. At all three times, the pressure falls significantly upstream of the stnoses and then increases with much lower magnitude downstream of the stenoses. The pressure variation magnitudes are much higher at the second stenosis compared with those happened at the first stenosis. Beyond the stenoses, the pressure increases to a value which is significantly lower than that at the inlet.

Wall shear stress is the tangential drag force produced by blood moving across the artery. It is a function of the velocity gradient of blood along the wall. Wall shear stress

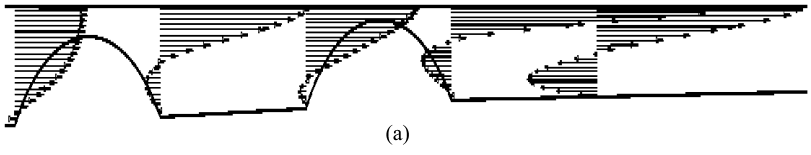

Figure 7.
Tapering effect on the velocity profiles in arteries: (a) tapering artery, (b) flat artery

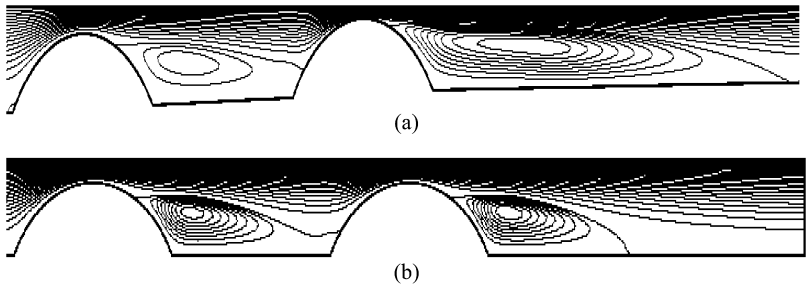

Figure 8.
Tapering effect on the streamlines of the flow fields in arteries: (a) tapering artery, (b) flat artery

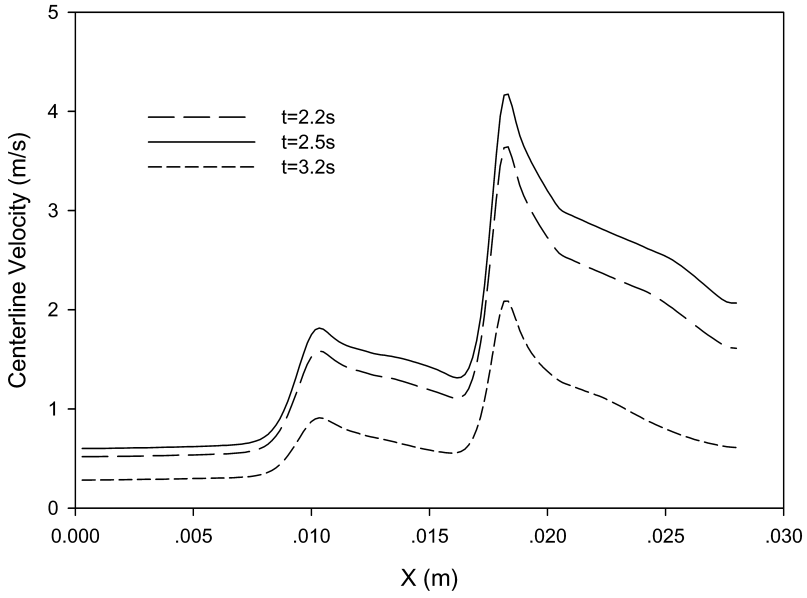

Figure 9.
Instantaneous centerline velocity profiles in the tapering artery with 90 percent stenoses

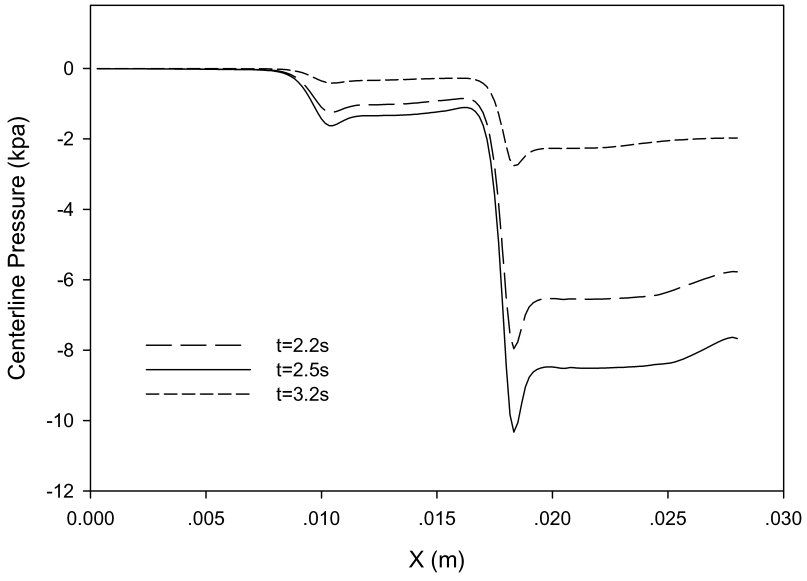

Figure 10.
Instantaneous centerline pressure profiles in the tapering artery with 90 percent stenoses

distributions for the 90 percent stenosis case are presented in Figure 11. It shows that the wall shear stress at the second stenosis reaches to maximum at the peak phase during the period cycle. Unlike the minimum pressure drop point, which occurred just downstream of the midpoint of the stenoses, the peak wall shear stress occurs at a location just upstream of the stenoses. This phenomenon was demonstrated in an analytical model presented by Young and Tsai (1973). Because of the stenotic severity,

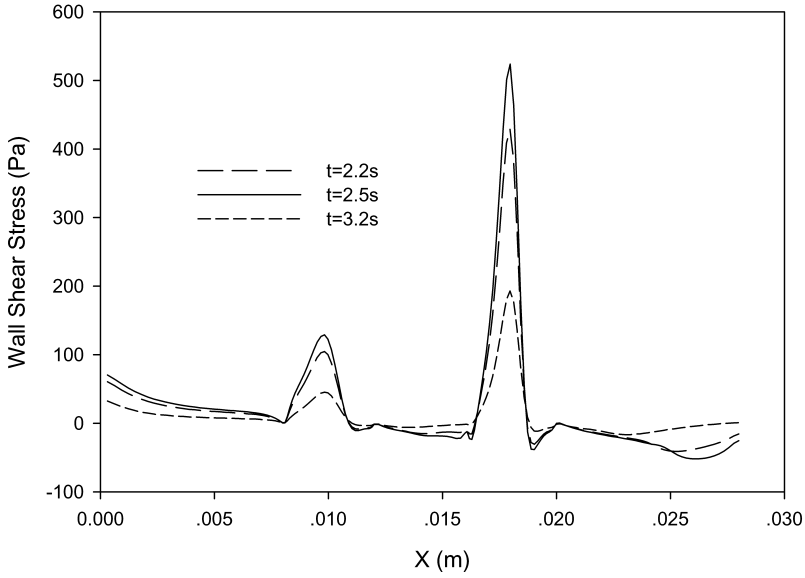

Figure 11.
Instantaneous distribution of wall shear stress in the tapering artery with 90 percent stenoses

the peak wall shear stress at the second stenosis is much higher than that at the first stenosis. At the upstream and downstream corners of the stenoses, wall shear stress is seen to approach zero, which implies the separation of the fluid flow.

Conclusions

Numerical predictions for turbulent pulsatile flow through two different axisymmetric stenoses were obtained within the framework of a two-equation turbulence model. The low Reynolds number $k - \omega$ model is applied to solve the governing equations. Under steady conditions, the effects of tapering and stenosis severity on the fluid flow are presented and compared. The turbulent flow is intensified and pressure falls more rapidly with the increasing stenosis severity. The recirculation zones are stretched and velocity profile varies more rapidly in the tapering artery compared with those in the flat artery. Under pulsatile conditions, the centerline velocity profile, pressure distribution and wall shear stress at accelerate, peak and decelerate phases are investigated. The maximums of velocity and wall shear stress and the minimum of pressure are reached at the peak phase. The variation of these three parameters is most significant at the peak phase.

References

Ahmed, S.A. (1998), "An experimental investigation of pulsatile flow through a smooth constriction", *Experimental Thermal and Fluid Science*, Vol. 17, pp. 309-18.

Ahmed, S.A. and Giddens, D.P. (1983a), "Velocity measurements in steady flow through axisymmetric stenoses at moderate reynolds number", *Journal of Biomechanics*, Vol. 16 No. 7, pp. 505-16.

Ahmed, S.A. and Giddens, D.P. (1983b), "Flow disturbance measurements through a constricted tube at moderate Reynolds numbers", *Journal of Biomechanics*, Vol. 16 No. 1, pp. 955-63.

Ahmed, S.A. and Giddens, D.P. (1984), "Pulsatile poststenotic flow studies with laser doppler anemometry", *Journal of Biomechanics*, Vol. 17, pp. 695-705.

Berger, S.A. and Jou, L.D. (2000), "Flows in stenotic vessels", *Annual Review of Fluid Mechanics*, Vol. 32, pp. 347-82.

Cao, J. and Rittgers, S.E. (1998), "Particle motion within in vitro models of stenosel internal carotid and left anterior descending coronary arteries", *Annals of Biomedical Engineering*, Vol. 26 No. 2, pp. 190-9.

Deshpande, M.D. and Giddens, D.P. (1980), "Turbulence measurements in a constricted tube", *Journal of Fluid Mechanics*, Vol. 97, pp. 65-89.

Friedman, M.H., Hutchins, G.M., Bargeron, C.B., Deters, O.J. and Mark, F.F. (1981), "Correlation between initial thickness and fluid shear in human arteries", *Atherosclerosis*, Vol. 39, pp. 425-36.

Ghalichi, F., Deng, X., De Champlain, A., Douville, Y., King, M. and Guidoin, R. (1998), "Low Reynolds number turbulence modeling of blood flow in arterial stenoses", *Biorheology*, Vol. 35 Nos. 4-5, pp. 281-94.

Giddens, D.P., Zarins, C.K. and Glagov, S. (1993), "The role of fluid mechanics in the localization and detection of atherosclerosis", *Journal of Biomechanical Engineering*, Vol. 115, pp. 588-94.

Holman, E. (1955), "The development of arterial aneurysms", *Journal of Surgical Gynecology Obstetrics*, Vol. 100, pp. 599-611.

Jung, J., Lyczkowski, R.W., Panchal, C.B. and Hassanein, A. (2006), "Multiphase hemodynamics simulation of pulsatile flow in a coronary artery", *Journal of Biomechanics*, Vol. 39, pp. 2064-73.

Ku, D.N. (1997), "Blood flow in arteries", *Annual Review of Fluid Mechanics*, Vol. 29, pp. 399-434.

Ku, D.N., Giddens, D.P., Zarins, C.K. and Glagov, S. (1985), "Pulsatile flow and atherosclerosis in the human carotid bifurcation, positive correlation between plaque location and low oscillating shear stress", *Arteriosclerosis*, Vol. 5, pp. 293-302.

Lee, T.S., Liao, W. and Low, H.T. (2003), "Numerical simulation of turbulent flow through series stenoses", *International Journal for Numerical Methods in Fluids*, Vol. 42 No. 7, pp. 717-40.

Li, M. X., Beech-Brandt, J.J., John, L.R., Hoskins, P.R. and Easson, W.J. (2007), "Numerical analysis of pulsatile blood flow and vessel wall mechanics in different degree of stenoses", *Journal of Biomechanics*, Vol. 40, pp. 3715-24.

Lieber, B. and Giddens, D.P. (1990), "Post-stenotic core flow behavior in pulsatile flow and its effects on wall shear stress", *Journal of Biomechanics*, Vol. 23, pp. 597-605.

Marshall, I., Zhao, S., Papathanasopoulou, P., Hoskins, P. and Xu, X.Y. (2004), "MRI and CFD studies of pulsatile flow in healthy and stenosed carotid bifurcation models", *Journal of Biomechanics*, Vol. 37, pp. 679-87.

Mittal, R., Simmons, S.P. and Udaykumar, H.S. (2001), "Application of large-eddy simulation to the study of pulsatile flow in modeled arterial stenosis", *Journal of Biomechanics*, Vol. 123, pp. 325-32.

Nguyen, K.T., Clark, C.D., Chancellor, T.J. and Papavassiliou, D.V. (2008), "Carotid geometry effects on blood flow and on risk for vascular disease", *Journal of Biomechanics*, Vol. 41, pp. 11-19.

Ojha, M., Cobbold, C., Johnston, K.W. and Hummel, R.L. (1989), "Pulsatile flow through constricted tubes: an experimental investigation using photochromic tracer methods", *Journal of Fluid Mechanics*, Vol. 203, pp. 173-97.

Pope, S.B. (2000), *Turbulent Flows*, Cambridge University Press, Cambridge.

Roshko, A. (1954), "On the development of turbulent wakes for votex streets", *NACA Report 1191*, pp. 124-32.

Scotti, A. and Piomelli, U. (2001a), "Numerical simulation of pulsating turbulent channel flow", *Physics of Fluids A*, Vol. 13 No. 5, pp. 1367-84.

Scotti, A. and Piomelli, U. (2001b), "Turbulence models in pulsating flow", AIAA Paper 2001-0729, pp. 1-11.

Stein, P.D. and Sabbah, H.N. (1976), "Turbulent blood flow in the ascending aorta of humans with normal and diseased aortic valves", *Circulation Reserach*, Vol. 39 No. 1, pp. 58-65.

Taber, L.A., Zhang, J. and Perucchio, R. (2007), "Computational model for the transition from peristaltic to pulsatile flow in the embryonic heart tube", *Journal of Biomechanical Engineering*, Vol. 129, pp. 441-9.

Varghese, S.S. and Frankel, S.H. (2003), "Numerical modeling of pulsatile turbulent flow in stenotic vessels", *Journal of Biomechanical Engineering*, Vol. 25 No. 4, pp. 445-60.

Wilcox, D.C. (1993), *Turbulence Modeling for CFD*, DCW industres, La Canada, CA.

Winter, D.C. and Nerem, R.M. (1984), "Turbulence in pulsatile flows", *Annals of Biomedical Engineering*, Vol. 12 No. 4, pp. 357-69.

Young, D.F. and Tsai, F.Y. (1973), "Flow characteristics in models of arterial stenoses-1. steady flow", *Journal of Biomechanics*, Vol. 6, pp. 395-410.

Corresponding author
Yuwen Zhang can be contacted at: zhangyu@missouri.edu